Two-Dimensional, Vision-Based μN Force Sensor for Microrobotics

David J. Cappelleri, Gianluca Piazza and Vijay Kumar

***Abstract*— We present a two-dimensional, vision-based force sensor, capable of sensing μN level forces. There are currently no reliable, off-the-shelf, commercially-available force sensors to measure forces at this scale, that can be easily integrated into standard microrobotic test-beds. Our design consists of a planar, elastic mechanism with known force-deflection characteristics. A CCD camera is used to track the deformation of the mechanism as it is used to manipulate objects in a micro/meso-scale robotic manipulation test-bed. By observing the displacements of select points in the mechanism, the manipulation forces can be estimated. The modeling, design, microfabrication, calibration and experimental validation of the force sensor are presented with a brief discussion of an application to a robotic manipulation tasks such as microassembly.**

I. INTRODUCTION

Force sensors at the micro-Newton (μN) scale are generally made using microfabrication technology. Traditional methods of indirect force measurements, like mounting strain gauges at specific locations [11], [28], are hard to demonstrate at the MEMS scale because they substantially complicate the micro-fabrication process. Methods like capacitance-based indirect force measurement usually require special electronic circuitry to measure the low capacitance of femto- and atto-farads and thus a complicated microfabrication process [2], [8], [23] that can drive up production costs results. Indeed there are no commercially-available, inexpensive, multi-axis force sensors at this scale that can be easily integrated with microrobotic manipulators. Our goal is to come up with a design that can be easily integrated into a microrobotic test-bed (Figure 1 (left) [5], [7]), which does not require any alteration of the object being manipulated or require exotic fabrication techniques or drive electronics and can sense μN level forces in two dimensions. With such a design, real-time controlled manipulation of micro-objects is possible. In this paper, we develop a two-dimensional (2D), computer vision-based, force sensing device which consists of an elastic mechanism with known force-deflection characteristics. From observing the deformation of a calibrated structure as it interacts with an object that it is manipulating, the actual manipulation force can be extracted.

The development of micro-force sensors has been an active research topic of late. An overview of force sensing for microassembly applications is given in [17] and a review of MEMS devices used for cellular force measurements can be found in [22]. The commercially available force sensor AE 801 Micro Force Sensor from SensorOne (*http://sensorone.com*) can measure forces from 12 grams down to 12 mg (118 mN to 118 μN) in one dimension. The Zyvex Force Characterization Package (FCP) (*http://www.zyvex.com*) is capable of measuring one dimensional forces ranging from nN to mN but requires extensive (proprietary) hardware, software, as well as a high resolution scanning electron microscope to function. An AFM is commonly used to measure smaller forces, in the pN to nN range [3]. Sitti et al. used an AFM for manipulation along with integrated force sensing at the mN level in [21]. Koch, et al. [15] designed, fabricated, and tested a compliant surface-micromachined spring in order to calibrate the lateral force field of an electromagnet on a single magnetic microparticle. Due to the high resolution microscope objective used, pN force sensitivity is achieved.

In regards to vision and optical force sensing, the design for a micrograting-based force sensor integrated with a surface micromachined silicon-nitride probe for penetration and injection into drosophila embryos is presented in [29]. Optics are also used in [30] and [12] to sense contact forces. A minimally intrusive, vision-based, computational force sensor for elastically deformable objects is presented in [25]. Force estimation is calculated from the visually measured displacements and known material properties of the deformable object. This approach is only viable if the displacements of the deforming object can be captured accurately. Greminger, et al. demonstrates a method to visually measure the force distribution applied to a linearly elastic object using the contour data in an image in [10]. Sasoglu, et al. have used high-aspect ratio polydimethylsiloxane (PDMS) microbeams to sense one dimensional micro-scale forces specifically targeted for single cell studies [19]. Similar PDMS beam structures have been used by Liu et al. [16] to hold a cell in place during microrobotic mouse embryo injection while tracking the beam displacements, thus extracting force information. A sub-pixel visual tracking algorithm allows for 3.7 nN force resolution.

Our design, which allows for two-dimensional sensing of micro-forces, can be easily integrated into standard robotic manipulation test-beds without cluttering the workspace or requiring any complicated drive electronics. It can also be used as a manipulation tool to execute a variety of tasks and is applicable to many different applications. The modeling, design, microfabrication, calibration and experimental validation of this force sensor are presented in the following sections along with a brief discussion of application to a robotic manipulation tasks such as microassembly.

This work was partially supported from NSF grants IIS-0427313, NSF IIP-0742304, and IIS-0413138, ARO grant W911NF-05-1-0219, and ONR grant N00014-07-1-0829. D. Cappelleri is from Stevens Institute of Technology, Hoboken, NJ USA dcappell@stevens.edu, V. Kumar and G. Piazza are from University of Pennsylvania, Philadelphia, PA USA {kumar, piazza}@seas.upenn.edu

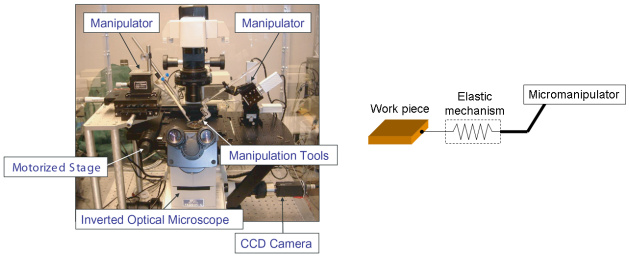

Fig. 1. Microrobotic test-bed (left); Force sensor design (right)

II. FORCE SENSOR DESIGN

The μN force sensor design presented here is intended for use in the micro/meso-scale robotic manipulation test-bed that is pictured in Figure 1 (left). For manipulation at these scales, surface forces, such as stiction, friction, and electrostatic forces, dominate. Most parts are planar so access to the parts from the top is generally possible. Grasping the part with a suction gripper is possible, however it can only be used to approximately position the parts due to the difficulties in part release resulting from dominate surface forces. Therefore, we use manipulators (probes) with one or more point contacts to position parts. The approach for the force sensor design can be seen schematically Figure 1(right). We want to design an elastic mechanism that can be directly mounted to the micro-manipulator at one end, while the other end can be used to manipulate parts by pushing on them with one or more point contacts. The device needs to be designed with geometry that can be tracked in two dimensions in the images from the CCD camera, providing two-dimensional (in the XY-plane) μN level force sensing. In order to maximize the field of view (FOV) of the microscope in the test-bed, we use a 4X objective. This leads to a vision system resolution $\simeq$ 5 μm/pixel. We want to minimize the μN/pixel ratio in order to achieve the maximum sensitivity for our device. For example, a desired resolution of 0.25 μN/pixel (or 4 pixels/μN) corresponds to a maximum stiffness in each direction of the device of 0.0475 N/m.

A. Approach

The design principles and formulas used to design compression springs are leveraged here to derive some intuitive designs for the vision-based force sensor. We essentially want to design a low stiffness, two-dimensional spring. In order to design a low stiffness spring/structure for a given design space and material, one needs to have many active coils and/or thin elastic members. These design principles have been utilized in the design of MEMS linear actuators, resonators, and accelerometers. Typically these suspension designs have large displacements in the direction of actuation and high stiffness in the other two perpendicular directions and consist of spring-like, elastic flexure elements in various configurations along with a centrally located rigid shuttle mass [18]. The *simple suspension* and *crab-leg* design topologies were initially explored here. The shuttle mass geometry was modified to include a rigid probe section to be used for manipulation. The beam geometries were designed for low stiffness in both the lateral and transverse directions (switching from low stiffness in 1D to 2D) and nonlinear finite element analysis (FEA) performed. The material was taken to be silicon and no constraints on the design domain size enforced. The results produced beam dimensions that yielded stiffness in the desired range needed to sense μN level forces. However, the aspect ratios of the beam length:width and beam length:thickness were very large. Thus, the out-of-plane stiffness was too low causing the device to deform under its own weight. In order to avoid this problem, the design space needed to be fixed in size and a more sophisticated way to minimize the 2D stiffness of the structure in the given design space had to be developed.

B. Silicon Designs $\Rightarrow$ PDMS Designs

The design methodology and procedure used to obtain the lowest stiffness design topology for a fixed design space is described in detail in [4] and is summarized in the following paragraphs. A Monte Carlo optimization of planar, spring-like structures, yielded a number of candidate designs. Macro-scale prototypes of these designs were manufactured out of acrylic using a laser cutter and the stiffness of each design in the *X*- and *Y*-direction were determined experimentally. Observations and conclusions were drawn from the experimental results which allowed for the designs to be refined by increasing the lengths of springs and changing their placements in order to provide even more improved (lower) stiffness values for a fixed design domain. Next, the dimensions of these macro-scale designs were scaled down to the micro-scale. Material properties for silicon were used to calculate corresponding stiffness values in the *X*- and *Y*-directions. While these designs did have much improved (lower) stiffness values than the original designs investigated and did not have the aspect ratio problems causing them to deform out-of-plane, the stiffness values were still not low enough to sense forces at the μN level. Therefore, we instead decided to use polydimethylsiloxane (PDMS) for the sensor design.

PDMS is a silicon-based organic polymer and is commonly used in microfluidic applications [13]. It is much softer than silicon (E_{PDMS} = 360 kPa to $\sim$3 MPa [1], [6] vs. $E_{silicon}$ = 160 GPa [20]) and using it for the designs instead of silicon allows for the minimum feature size of the devices to be increased for easier manufacturing while decreasing the overall footprint for the device to attain the same desired stiffness. Figure 2 shows a schematic of a macro-scale prototype design that has a combination of both low *X* and *Y* stiffness values as well as high out-of-plane stiffness that was used as a starting point to optimize the PDMS structures. This design is parameterized by a set of parameters that provide a geometric description for the design, also shown in the figure. The only parameter not defined in this figure is t_z, the out-of-plane beam thickness. This design is symmetric about the *Y*-axis and consists of a series of springs with varying number of turns (n) and link lengths (L_i's). A design parameter study was performed to come up with a set of feasible designs. For each design scenario considered, a linear finite element analysis was used

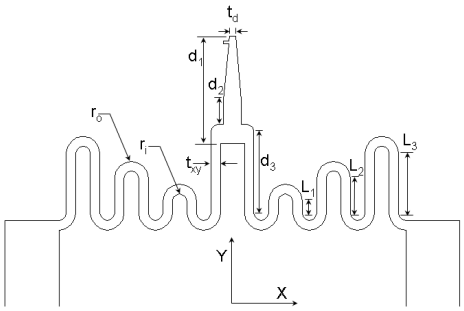

Fig. 2. PDMS prototype design parameters

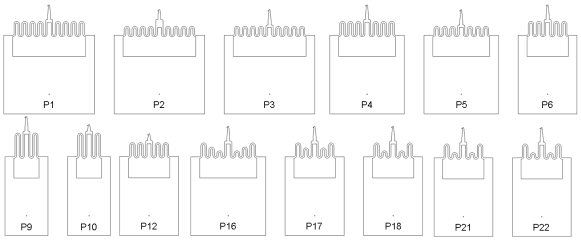

Fig. 3. PDMS Prototype Designs

to predict theoretical stiffness values in both the *X*- and *Y*-directions. Fourteen designs were identified to meet the design requirement of 0.0475 N/m maximum stiffness along each direction. The corresponding geometric descriptions for these designs are presented in Table I along with their stiffness values.

III. Force Sensor Fabrication

Microfabricating these force sensor designs out of PDMS requires a more complicated manufacturing process than if they were to be made just out of silicon. A mold first needs to be created that the PDMS material can be poured into, allowed to cure, and then the parts released or extracted from. The microfabrication process begins with spin-coating KMPR 1050 negative photoresist (MicroChem, *www.microchem.com*) onto a clean silicon wafer (Figure 4(a)) followed by soft-baking on a hot plate for 30 minutes @ 105^oC. A corresponding negative mask was then used in the photolithography step (Figure 4(b)). The mask defines the geometry of the entire device (base, spring, and tip sections). The wafer and mask were then exposed to 365 nm, 5 mW/cm^2 intensity, UV light with soft-contact for 3 minutes and then a post-exposure bake (PEB) @ 105^oC for 4 min 15 sec was administered to the wafer. In order to help with the release of the cured PDMS device, the patterned wafer was then exposed to CF_4 plasma for 1 minute using a RIE machine [14](Figure 4(d)). PDMS (Dow Corning Sylgard 184 elastomer base and curing agent, *www.dowcorning.com*) was mixed with a base:cure ratio of 12.5:1 (by weight) and then spin-coated onto the wafer, Figure 4(e), and cured. The curing procedure presented in [13] was modified to include clamping of the patterned wafer with PDMS between two aluminum plates with four C-clamps, one at each corner, and placing it in an oven for 3 hours at 100^oC. It was then allowed to cool overnight back down to room temperature before clamp removal. The planarization of the PDMS shown in Figure 4(f) was then performed with wet etching. Examples of wet etching of PDMS can be found in [9] [27] [24] and a similar recipe was used here. A solution of tetrabutylammonium fluoride (TBAF) in N-Methylpyrrolidinone (NMP) (3:1; v/v; NMP/75%TBAF in water) was used as the PDMS etchant. The wafer was submerged in the solution for 10 minutes and then placed in a DI water bath for 3 minutes. After planing the PDMS, the photoresist (KMPR) was dissolved by placing the wafer in Remover-PG (MicroChem) solution for about 30 minutes while in a sonicator @ 60^oC, Figure 4(g). The wafer was then placed in an acetone bath for approximately 20 hours to swell the PDMS parts and make their extraction easier. The parts were then extracted by peeling them off the wafer with tweezers, Figure 4(h). Beryllium copper bases for the devices were manufactured with a photochemical machining process, courtesy of Fotofab (*www.fotofab.com*). They have nominal dimensions of 2.3 mm x 2.3 mm x 152.4 μm and are used to provide rigidity to the base (handle) portion of the device. These base parts were epoxied to the base section of the PDMS force sensor, which was then epoxied to the end of a tungsten probe, completing the fabrication process (Figure 4(i)).

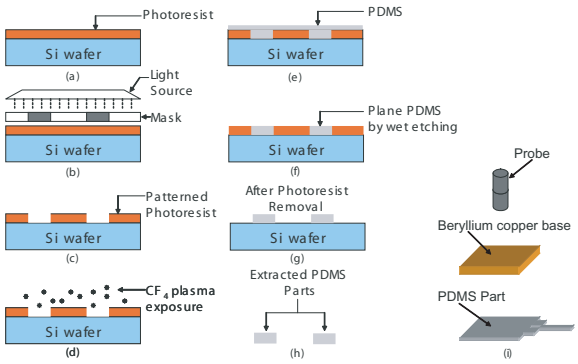

Fig. 4. Microfabrication Process

Subassemblies, consisting of the beryllium copper bases

TABLE I

Prototype Geometric Descriptions and Stiffness Values

Design	n	L_1 (μm)	L_2 (μm)	L_3 (μm)	L_4 (μm)	d_1 (μm)	d_2 (μm)	d_3 (μm)	k_x (N/m)	k_y (N/m)
P1	4	250	250	250	250	450	100	340	0.0007	0.0010
P2	4	125	125	125	125	450	100	340	0.0033	0.0037
P3	4	125	125	125	125	450	100	200	0.0032	0.0036
P4	3	250	250	250	–	450	100	340	0.0023	0.0053
P5	3	125	125	125	–	450	100	200	0.0042	0.0078
P6	2	250	250	–	–	450	100	340	0.0033	0.0144
P9	1	500	–	–	–	450	100	590	0.0023	0.0266
P10	1	500	–	–	–	250	50	590	0.0036	0.0500
P12	2	250	250	–	–	250	50	340	0.0064	0.0144
P16	3	50	145	250	–	450	100	340	0.0025	0.0060
P17	2	125	250	–	–	450	100	340	0.0033	0.0149
P18	2	50	250	–	–	450	100	340	0.0034	0.0152
P21	2	35	250	–	–	450	100	340	0.0035	0.0152
P22	2	30	250	–	–	450	100	340	0.0035	0.0153

Constants: r_i = 30 μm, $r_o = r_i + t_{xy}$, t_d = 25 μm, t_{xy} = 40 μm, t_z = 50 μm

Material Properties: E_{PDMS} = 615 kPa, ν = 0.48

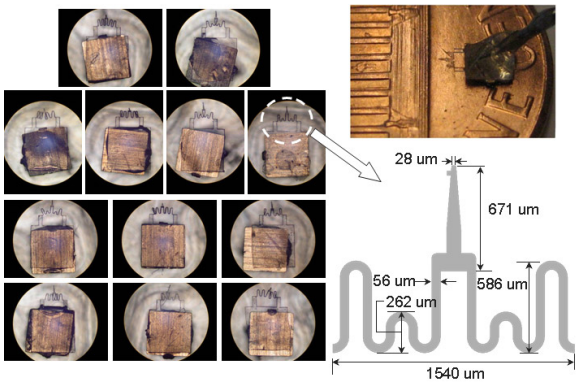

Fig. 5. Prototype subassemblies and selected prototype schematic

TABLE II

GEOMETRIC DESCRIPTION FOR FABRICATED PDMS PROTOTYPE

Design	n	L_1 (μm)	L_2 (μm)	L_3 (μm)	L_4 (μm)	d_1 (μm)	d_2 (μm)	d_3 (μm)
Proto P18	2	60	384	–	–	671	147	502

Constants: r_i = 45 μm, $r_o = r_i + t_{xy}$, t_d = 28 μm
t_{xy} = 56 μm, t_z = 176 μm

and extracted PDMS parts, are shown in Figure 5 (left). Note: the thicker the part is, the easier it is to remove it from the substrate. Therefore, PDMS parts thicker than the design value (50 μm) were fabricated. This was also done to compensate for the unknown wet etch rates a priori. The thicker the PDMS parts, the stiffer the force sensor. Since the finite element analysis on the original design geometries predicted stiffnesses much lower than the required stiffness values, increasing the thickness of the devices will still produce force sensors that meet the stiffness requirement. One of the subassemblies from Figure 5 is shown in more detail on the right side of the figure. Table II lists all of the measured design parameters for this prototype. These dimensions most closely resemble those of design P18 from Table I. A tungsten probe was fastened to the prototype subassembly with epoxy, completing the fabrication process.

IV. CALIBRATION AND MODELING

A. Material Testing

This stiffness of the prototype is determined by the part geometry and PDMS material properties. The Poisson's ratio for PDMS is known to be ≈0.5 [1]. The elastic modulus has a known range of 360 kPa to 3 MPa which varies based on curing agent:base solution ratio as well as other processing parameters and therefore needs to be tested for on a per wafer basis. PDMS samples from the same wafer as *Proto P18* without spring and tip sections were used for material property tests. The modulus of elasticity of these samples were tested for with compression tests on an Instron 4206 machine and 10 N load cell. The samples started with a slight pre-load and then were loaded up to 45g (∼440 mN). Three samples were tested three times each and their corresponding stress-strain curves plotted in which the slopes yield the elastic modulus values for the particular sample. The average elastic modulus for the samples was taken as the elastic modulus for the device, 333.4 KPa. This value is at the low end of the range of published values for E_{PDMS}.

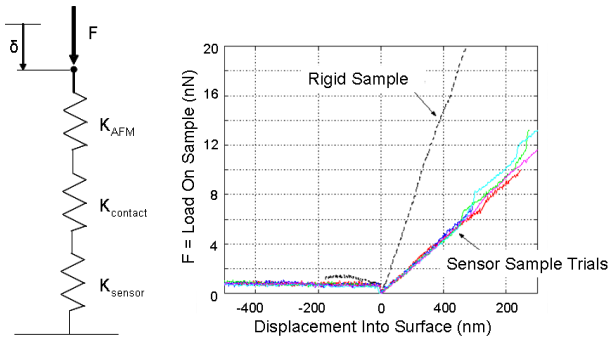

(a) Model (b) Force-distance curves

Fig. 6. AFM calibration tests

B. AFM Nanoindentation Tests

Atomic force microscope (AFM) nanoindentation tests were also performed on the prototype to determine it's horizontal and vertical stiffness values. A calibrated AFM cantilever was used to apply a known force to the device that is mounted below it. The cantilever was first lowered to contact a rigid sample to determine the deflection sensitivity of the cantilever. From knowing this and the cantilever stiffness (K_{AFM}), this displacement data was converted to force data to create a force-distance curve.

The system can be modeled as three springs in series, as shown in Figure 6(a), and the value for the stiffness of the device directly calculated from the AFM test data and the equation:

$$\delta = (1/K_{AFM} + 1/K_{contact} + 1/K_{sensor})F \qquad (1)$$

where δ is the photodiode displacement, F is the load applied to the sample, K_{sensor} is the sensor stiffness, K_x or K_y, depending on the mounting orientation, and $K_{contact}$ = contact stiffness for PDMS. K_{AFM} is known from calibration and δ and F are results from the indentation test data. The contact stiffness was first solved for by conducting an indentation test on a thick PDMS substrate section of the device so that $K_{sensor} = 0$ and $K_{contact}$ can be directly solved for.

Separate tests were performed to determine K_{sensor}, corresponding to K_x and K_y. At least 5 trials for each test were performed and force-distance curves were plotted for the compliant samples on the same axes as the data from a rigid sample to extract the corresponding δ and F values. The force-distance curves from the horizontal stiffness tests are shown in Figure 6(b). These tests produced stiffness values of K_x = 0.0365 N/m and K_y = 0.0660 N/m. FEA of the prototype using E_{PDMS} from the compression tests and the measured part geometry (Table II) yielded stiffness values with roughly the same K_y/K_x ratio as the AFM calibration tests but with much lower stiffness values: K_x = 0.00282 N/m and K_y = 0.00675 N/m. This discrepancy in stiffness values between the finite element model and the AFM tests can be attributed to misalignment between the AFM tip and sensor angles and the facts that (1) the PDMS has a nonlinear stiffness that depends very much on the loading force range and (2) nanoindentation tests are known to produce higher material siffnesss values than traditional compression

test results for PDMS [26]. The AFM indentation tests done here correspond to a very low loading force range (nN). Differently, the loads from the compression tests are in the μN to mN range. Therefore, it is reasonable that stiffness values from the nanoindentation tests are much higher. Since the device will not be operating in such a low force regime, the E_{PDMS} from the compression tests, corresponding to the lower device stiffness values, were used in finite element models to determine the force-displacement relationship for the device while subjected to μN loads at various angles in the XY-plane.

C. Calibration Curves

We conducted finite element analysis (FEA) with various loads at varying angles applied to the tip of the device. Displacement values corresponding to tracking points $N_t = (X_t, Y_t)$, $N_b = (X_b, Y_b)$, and $N_{tip} = (X_{tip}, Y_{tip})$ in Figure 7(a) were recorded for each run. The displacement data for all three nodes for the various runs was compiled in both μm and in corresponding image pixels. This FEA data was used to compute a quadratic calibration curve for the force sensor in the form of:

$$F = \beta_0 + \beta_1(\Delta X) + \beta_2(\Delta Y) + \beta_{12}(\Delta X)(\Delta Y) + \beta_{11}(\Delta X^2) + \beta_{22}(\Delta Y^2) \quad (2)$$

where F is either the *X*- or *Y*-direction force, F_x or F_y, and ΔX and ΔY correspond to displacements of a particular node of interest. The FEA data was first transformed to the image coordinate system to correspond to displacement components for the nodes of interest: ΔX_t, ΔY_t, ΔX_b, ΔY_b, ΔX_{tip}, and ΔY_{tip} (in pixels) and forces F_x and F_y (μN) according to the axes shown in Figure 7(a). Matlab® was used to perform regression analysis and solve for the unknown β terms, which vary with the different choices for the input variables, with a 99% confidence interval.

V. MICROMANIPULATION EXPERIMENTS

The fully assembled prototype was mounted to the 4-axis computer controlled manipulator in the experimental test-bed shown in Figure 1 (left) to test the viability of the prototype for micro- and meso-scale assembly tasks. Meso-scale beryllium copper parts were placed on a glass microscope slide and experimental test pushes with the force sensor on the parts executed. Figure 7(b) shows the force sensor about to push one of the test parts while Figure 8 shows screen shots from two test pushes executed back-to-back in the system test-bed. In order to extract force information from the captured images, the displacements of the device in each image frame needed to be tracked accordingly. Four tracking points on the prototype force sensor were designated for tracking and are shown in Figure 7(a). Points N_t, N_b, and N_{tip} move when force is applied at the tip. Point $N_f = (X_f, Y_f)$ is a fixed position on the device that doesn't change when the tip encounters a force. By tracking the positions of any of the moving points along with a fixed point in each image frame, displacement data for the device is extracted. Image processing was performed to extract this information

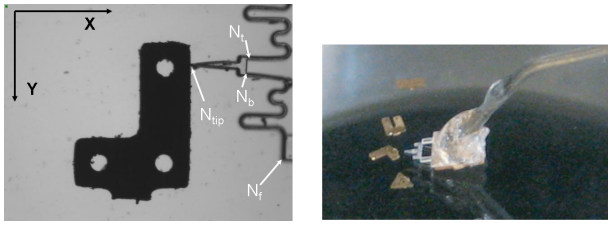

(a) Image tracking points (b) Force sensor pushing part

Fig. 7. Micromanipulation experiments

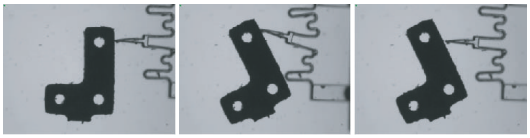

(a) Test push 1: Initial, intermediate, and final configurations

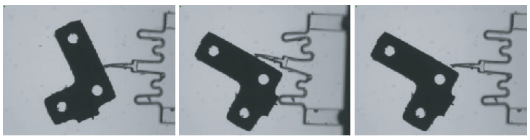

(b) Test push 2: Initial, intermediate, and final configurations

Fig. 8. Snapshots from experimental test pushes

for these two test pushes. Three models, corresponding to each tracking point's displacement data, were created to calculate the *X*- and *Y*-direction forces corresponding to the two test pushes. The orientation of the part was also tracked and used to convert the *X*- and *Y*-component forces to normal (*n*-) and tangential (*t*-) directional forces. The results from all the models were consistent and in the expected force range for pushing the part from rest. The maximum *n*-direction force required to move the part in the first push was approximately 1.5 μN, while it was 2.0 μN for the second push. There are also high tangential forces required to overcome the surface frictional forces between the metal part and glass substrate, 1.2 μN and 2.4 μN, respectively. This makes sense since that in push 2, the pushing location was more centrally located, closer to the center of mass of the part, causing more of a translational motion of the part and requiring larger forces.

The performance of the force sensor can now be evaluated against the design requirements. These design requirements were stated earlier as trying to minimize the μN/pixel ratio, with $K_x, K_y \leq$ 0.0475 N/m, corresponding to a resolution of 0.25 μN/pixel (4 pixels/μN). FEA of the prototype, with the measured dimensions and E_{PDMS} from the compression tests, yielded stiffness values of K_y = 0.00282 N/m and K_x = 0.00675N/m. This was calculated as the ratio of the applied force and the displacement of the sensor tip. In this application, displacements of points N_t or N_b were tracked instead of the tip displacements. The stiffness values corresponding to the applied force divided by the displacements at either of these locations are K_y = 0.0136 N/m and K_x = 0.00738 N/m, respectively, corresponding to 14 and 26 pixels/μN resolution along each axis. Thus, the designed and fabricated prototype does indeed meet the design requirements.

VI. CONCLUSIONS

A proof-of-concept prototype of a compliant mechanism, vision-based force sensor has been described in this paper. The sensor does not require any additional instrumentation to be added to the microrobotic manipulation test-bed and can be used to sense both displacements and forces as well as used as a manipulation tool. We performed experimental tests and FE modeling in order to benchmark and calibrate a microfabricated PDMS prototype. Absolute calibration of the device is hard because of the difficulties in characterizing soft, viscoelastic materials like PDMS.

Extensive experimentation needs to be conducted before this device can be turned into a commercial product. The repeatability for the sensor needs to be quantified as well as some measure of the life cycle for a particular sensor identified from testing multiple prototypes. Our future work is in both of these areas and in designing structures with decoupled displacements at the tracking points. Never-theless, this proof-of-concept design is the first step in producing a viable, low cost, commercial product that can be easily integrated into standard micromanipulation systems to sense 2D μN level forces in microrobotic applications.

VII. ACKNOWLEDGMENTS

We gratefully acknowledge the support of NSF Grant IIS-0413138, Dept. of Education GAANN Grant P200A060275, and the Keck Foundation; Joe Grogan for his help in the microfabrication of the force sensor prototypes at the Wolf Nanofabrication Lab, University of Pennsylvania, and Prof. Robert Carpick and Graham Wabiszewski for discussions regarding the AFM calibration tests and help with and use of the Quesant AFM in the Carpick Research Group lab.

REFERENCES

[1] D. Armani, C. Liu, and N. Aluru. Re-configurable fluid circuits by pdms elastomer micromachining. In *Twelfth IEEE International Conference on Micro Electro Mechanical Systems (MEMS)*, Orlando, FL, Jan 17-21 1999.

[2] F. Beyeler, A. Neild, S. Oberti, D. Bell, Y. Sun, J. Dual, and B. Nelson. Monolithically fabricated micro-gripper with integrated force sensor for manipulating micro-objects and biological cells aligned in an ultrasonic field. *IEEE/ASME Journal of Microelectromechanical Systems (JMEMS)*, 16(1):7–15, February 2007.

[3] H.-J. Butt, B. Cappella, and M. Kappl. Force measurements with the atomic force microscope: Technique, interpretation and applications. *Surface Science Reports*, 59:1–152, 2005.

[4] D. Cappelleri. *Flexible Automation of Micro and Meso-Scale Manipulation Tasks with Applications to Manufacturing & Biotechnology*. Ph.d. dissertation, University of Pennsylvania, Philadelphia, PA, August 2008.

[5] D.J. Cappelleri, J. Fink, B. Mukundakrishnan, V. Kumar, and J.C. Trinkle. Designing open-loop plans for planar micro-manipulation. *IEEE Int. Conf. on Robotics and Automation, Orlando, FL*, May 2006.

[6] F. Carrillo, S. Gupta, M. Balooch, S. Marshall, G. Marshall, and L. Pruitt adn C. Puttlitz. Nanoindentation of polydimethylsiloxane elastomers: Effect of crosslinking, work of adhesion, and fluid environment on elastic modulus. *Journal of Materials Research*, 20(10):2820–2830, October 2005.

[7] P. Cheng, D. Cappelleri, B. Gavrea, and V. Kumar. Planning and control of meso-scale manipulation tasks with uncertainties. In *Proceedings of Robotics: Science and Systems*, Atlanta, GA, USA, June 2007.

[8] E. Enikov and B. Nelson. Three-dimensional microfabrication for a multi-degree-of-freedom capacitive force sensor using fibre-chip coupling. *Journal of Micromech. Microeng.*, 10:492–497, 2000.

[9] J. Garra, T. Long, J. Currie, T. Schneider, R. White, and M. Paranjape. Dry etching of polydimethylsiloxane for microfluidic systems. *J. Vac. Sci. Technol. A*, 20(3):975–982, May/June 2002.

[10] M. Greminger and B. Nelson. Vision-based force measurement. *IEEE Transactions on Pattern Analysis and Machine Intelligence*, 26(3):290–298, March 2004.

[11] A. Hoover and R. Fearing. Rapidly prototyped orthotweezers for automated microassembly. In *IEEE Int. Conf. on Robotics and Automation (ICRA)*, Rome Italy, April 2007.

[12] K.-H. Jeong, C. Keller, and L. Lee. Direct force measurements of biomolecular interactions by nanomechanical force gauge. *Applied Physics Letters*, 86(19), 2005.

[13] B. Jo, L. Lerberghe, K. Motsegood, and D. Beebe. Three-dimensional micro-channel fabrication in polydimethylsiloxane (PDMS) elastomer. *Journal of Microelectromechanical Systems*, 9(1):76–81, March 2000.

[14] J. Kim, J. Park, S. Yang, J. Baek, B. Kim, S.H. Lee, E-S. Yoon, K. Chunb, and Sukho Park. Establishment of a fabrication method for a long-term actuated hybrid cell robot. *Lab on a Chip*, 7:1504–1508, 2007.

[15] S. Koch, G. Thayer, A. Corwin, and M. de Boer. Micromachined piconewton force sensor for biophysics investigations. *Applied Physics Letters*, 89(173901), 2006.

[16] X. Liu, K. Kim, Y. Zhang, and Y. Sun. Nanonewton force sensing and control in microrobotic cell manipulation. In *Proceedings of Robotics: Science and Systems IV*, Zurich, Switzerland, June 2008.

[17] B. Nelson, Y. Zhou, and B. Vikramaditya. Sensor-based microassembly of hybrid MEMS devices. *IEEE Control Systems Magazine*, 18(6):pp. 35 – 45, December 1998.

[18] L. Saggere, S. Kota, and S.D. Crary. A new design for suspension of linear microactuators. *Proc. of the International Mechanical Engineering Congress and Exposition: Dynamic Systems and Control, Chicago, IL, ASME DSC*, 55(2):671675, 1994.

[19] F. Sasoglu, A. Bohl, and B. Layton. Design and microfabrication of a high-aspect-ratio pdms microbeam array for parallel nanonewton force measurement and protein printing. *Journal of Micromechanics and Microengineering*, 17:623–632, 2007.

[20] S. Senturia. *Microsystem Design*. Kluwer Academic Publishers, Boston, MA, 2003.

[21] M. Sitti. Teleoperated and automatic nanomanipulation systems using atomic force microscope probes. In 42^{nd} *IEEE Conference on Decision nad Control*, Maui, Hawaii USA, December 2003.

[22] Y. Sun and B. Nelson. MEMS for cellular force measurements and molecular detection. *International Journal of Information Acquisition*, 1(1):23–32, 2004.

[23] Y. Sun, B. Nelson, D. Potasek, and E. Enikov. A bulk microfabricated multi-axis capacitive cellular force sensor using transverse comb drives. *Journal Of Micromechanics And Microengineering*, 12(832-840), 2002.

[24] S. Takayama, E. Ostuni, X. Qian, J. McDonald, X. Jiang, P. LeDuc, M-H. Wu, D Ingber, and G. Whitesides. Topographical micropatterning of poly(dimethylsiloxane) using laminar flows of liquids in capillaries. *Advanced Matter*, 13(8):570–574, April 2001.

[25] X. Wang, G.K. Ananthasuresh, and J. Ostrowski. Vision-based sensing of forces in elastic objects. *Sensors and Actuators A*, 94:142–156, 2001.

[26] C. White and R. Drzal. Viscoelastic characterization of polymers using dynamic instrumented indentation. *Mater. Res. Soc. Symp. Proc.*, 841:R5.3.1–R5.3.6, 2005.

[27] B. Xu, F. Arias, and G. Whitesides. Making honeycomb microcomposites by soft lithography. *Advanced Matter*, 11(6):492–495, 1999.

[28] Y. Yamamoto, R. Konishi, Y. Negishi, and Tatsuo Kawakami. Prototyping ubiquitous micro-manipulation system. In *Proceedings of the IEEE International Conference on Advanced Intelligent Mechatronics (AIM)*, 2003.

[29] X. Zhang, C.-C. Chen, R. Bernstein, S. Zappe, M. Scott, and Olav Solgaard. Microoptical characterization and modeling of positioning forces on drosophila embryos self-assembled in two-dimensional arrays. *Journal of Microelectromechanical Systems*, 14(5):1187–1197, October 2005.

[30] Y. Zhou and B. Nelson. The effect of material properties and gripping force on micrograsping. In *Proceedings of the IEEE International Conference on Robotics & Automation (ICRA)*, San Francisco, CA, April 2000.